Orbit-induced localized spin angular momentum in strong focusing of optical vectorial vortex beams

Manman Li,[1,2] Yanan Cai,[1,2] Shaohui Yan,[1,*] Yansheng Liang,[1,2] Peng Zhang,[1] and Baoli Yao[1,†]
[1]*State Key Laboratory of Transient Optics and Photonics, Xi'an Institute of Optics and Precision Mechanics, Chinese Academy of Sciences, Xi'an 710119, China*
[2]*University of Chinese Academy of Sciences, Beijing 100049, China*

(Received 14 September 2017; revised manuscript received 12 March 2018; published 29 May 2018)

Light beams may carry optical spin or orbital angular momentum, or both. The spin and orbital parts manifest themselves by the ellipticity of the state of polarization and the vortex structure of phase of light beams, separately. Optical spin and orbit interaction, arising from the interaction between the polarization and the spatial structure of light beams, has attracted enormous interest recently. The optical spin-to-orbital angular momentum conversion under strong focusing is well known, while the converse process, orbital-to-spin conversion, has not been reported so far. In this paper, we predict in theory that the orbital angular momentum can induce a localized spin angular momentum in strong focusing of a spin-free azimuthal polarization vortex beam. This localized longitudinal spin of the focused field can drive the trapped particle to spin around its own axis. This investigation provides a new degree of freedom for spinning particles by using a vortex phase, which may have considerable potentials in optical spin and orbit interaction, light-beam shaping, or optical manipulation.

DOI: 10.1103/PhysRevA.97.053842

I. INTRODUCTION

In addition to energy and linear momentum, angular momentum (AM) is another important attribute of light beams [1]. Generally speaking, photons may have two different types of AM: optical spin angular momentum (SAM) and optical orbital angular momentum (OAM). The former is related to the state of polarization of light beams, left- and right-circular polarizations usually being thought as its two eigenstates [2]. The latter, OAM, is associated with the helical wave front of light beams, namely, a vortex phase structure $\exp(im\phi)$ (m is the topological charge and ϕ is the azimuthal angle) [3]. When interacting with a small particle, the optical SAM or OAM of light beam can transfer to the particle, resulting in the particle spinning around its own axis [4–6] or orbiting around the beam axis [7–9]. Such intriguing mechanical effects have been widely used in applications regarding light-matter interactions like optical manipulations [10,11], biology [12], and optomechanical systems [13].

Although optical SAM and OAM are two different rotation degrees of freedom of light beams that are nearly independent, they can be strongly coupled under some specific conditions such as light-matter interaction in inhomogeneous [14], anisotropic [15], or structured media [16], focusing or scattering of a circularly polarized beam [17]. This AM interacts, appearing between the spin and orbital terms, called optical spin-orbit interaction (SOI), which has attracted intensive attention recently for its novel fundamental and emerging applications [18–20]. The main SOI phenomena in optics cover: spin-Hall effects in inhomogeneous media [21], spin-dependent effects in nonparaxial fields [22], spin-controlled shaping of light using anisotropic structures [23], as well as spin-directional coupling via evanescent near fields [24]. These SOI phenomena, however, involve only the spin affecting and controlling on the spatial structure of phase of light beams [14–24].

One would expect that the inverse phenomenon can take place. But, there were no previous proposals showing the OAM to SAM conversion, which is still an open question. In this paper, we show the spatial phase structure of light beam can induce a localized spin by strongly focusing an azimuthal polarization vortex (APV) beam. As we know, when a paraxial beam is highly focused, the initial paraxial SAM or OAM will be redistributed between the nonparaxial SAM and OAM in the focal field due to the conservation of total AM [25,26]. For example, tightly focusing a circular polarization (CP) beam, the SAM of the incident beam will be partly transferred into the OAM of the focused field, characterized by the vortex phase on the axial field [22]. Here, we propose to adopt the APV beam (with nonzero OAM) as the input field. Even though the total SAM is zero, the focused field, focused by a high-numerical-aperture (NA) objective lens, has the localized longitudinal SAM, arising from its purely transverse field structure that has a $\pi/2$ phase difference between the radial and azimuthal components. When considering trapping particles, the focused field of APV tends to induce an axial spinning motion of the trapped particle. The focusing properties of the APV beams have been reported in the literature at both theoretical and experimental levels [27–29]. This paper focuses on the AM interaction and transfer in the focusing process and the light-matter interaction. The influences of different parameters, such as the sign of the topological charge, the ratio of the pupil radius to the beam waist of the input beam, and the characteristics of the particle, on the SAM density and the optical torque are presented.

II. FOCUSING OF AZIMUTHAL POLARIZATION VORTEX BEAMS

The focusing of incident vector beams under a high-NA objective lens can be numerically analyzed with the

*shaohuiyan@opt.ac.cn
†yaobl@opt.ac.cn

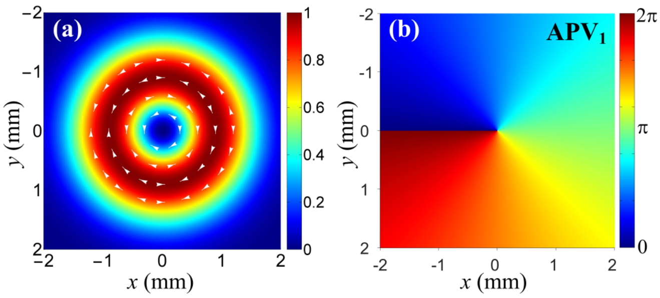

FIG. 1. Intensity (a) and phase (b) distributions in the entrance pupil plane of incident APV$_1$ beam. The white lines with arrows in (a) indicate the local polarization directions.

Richards-Wolf vectorial diffraction method [30,31]; then, the focused electric field in the vicinity of the focus can be expressed in an integral as

$$\mathbf{E}(\mathbf{r}) = \frac{-ikf}{2\pi}\int_0^{\vartheta}\int_0^{2\pi}\mathbf{A}(\theta,\phi)\exp(i\mathbf{k}\cdot\mathbf{r})\sin\theta d\phi d\theta, \quad (1)$$

where k is the wave number in the image space and f is the focal length; ϑ is the maximal converging angle determined by the NA; vectors $\mathbf{r}$ and $\mathbf{k}$ separately designate the observation point position in the image space and the wave vector of the refracted rays (focused by the objective lens); and $\mathbf{A}(\theta,\ \phi)$ stands for the apodized field, which is related to the input field $\mathbf{A}_0(\theta,\phi)$ at the entrance pupil according to the transform rule [32]

$$\mathbf{A}(\theta,\phi) = (\cos\theta)^{1/2}\begin{bmatrix}\mathbf{e}_\theta & 0\\ 0 & \mathbf{e}_\phi\end{bmatrix}\begin{pmatrix}A_{0\rho}\\ A_{0\phi}\end{pmatrix}, \quad (2)$$

where $(\mathbf{e}_\theta,\mathbf{e}_\phi)$ are the unit vectors in the θ and ϕ directions, respectively, and $(A_{0\rho},A_{0\phi})$ are the radial and azimuthal components of the input field $\mathbf{A}_0(\theta,\phi)$. For the APV beam discussed here, the input field can be written as the product of the amplitude, phase, and polarization vector as

$$\mathbf{A}_0(\theta,\phi) = \left(\beta_0\frac{\sin\theta}{\sin\vartheta}\right)^{|m|}\exp\left[-\beta_0^2\left(\frac{\sin\theta}{\sin\vartheta}\right)^2\right]\exp(im\phi)\mathbf{e}_\phi, \quad (3)$$

where β_0 is the ratio of the pupil radius and the beam waist; $\mathbf{e}_\phi$ is the unit vector in azimuthal direction in the input plane. Obviously, the input field has no SAM, carrying only the OAM of $m\hbar$ per photon.

Integrating along the azimuthal direction in (1), it is found that the axial field vanishes and the transverse field components (E_ρ,E_ϕ), in cylindrical coordinates (ρ_s,ϕ_s,z_s), are

$$\begin{Bmatrix}E_\rho\\ E_\phi\end{Bmatrix} = Ci^m e^{im\phi_s}\int_0^{\vartheta}\cos^{1/2}\theta\sin\theta A_0(\theta)e^{ikz_s\cos\theta} \times\begin{Bmatrix}i[J_{m+1}(\beta)+J_{m-1}(\beta)]\\ J_{m+1}(\beta)-J_{m-1}(\beta)\end{Bmatrix}d\theta. \quad (4)$$

Here $C = kf/2$ and $\beta = k\rho_s\sin\theta$; $A_0(\theta)$ denotes the amplitude function of the input field (3), $J_m(\beta)$ is the mth-order Bessel function of the first kind. We see that the focused field is purely transverse in polarization, with a radial field component more than an azimuthal component only, compared to the focused field of a commonly azimuthal polarization (AP) beam [31], due to the vortex phase structure of the incident field.

The intensity and phase profiles in the entrance pupil plane of the incident APV$_1$ beam are plotted in Fig. 1. The focal field of the incident APV$_1$ and APV$_{-1}$ beams passing through a high-NA ($= 1.26$) objective lens are calculated in Fig. 2, where the subscripts represent the sign and value of the topological charge m. The incident power is assumed to be $P = 100$ mW,

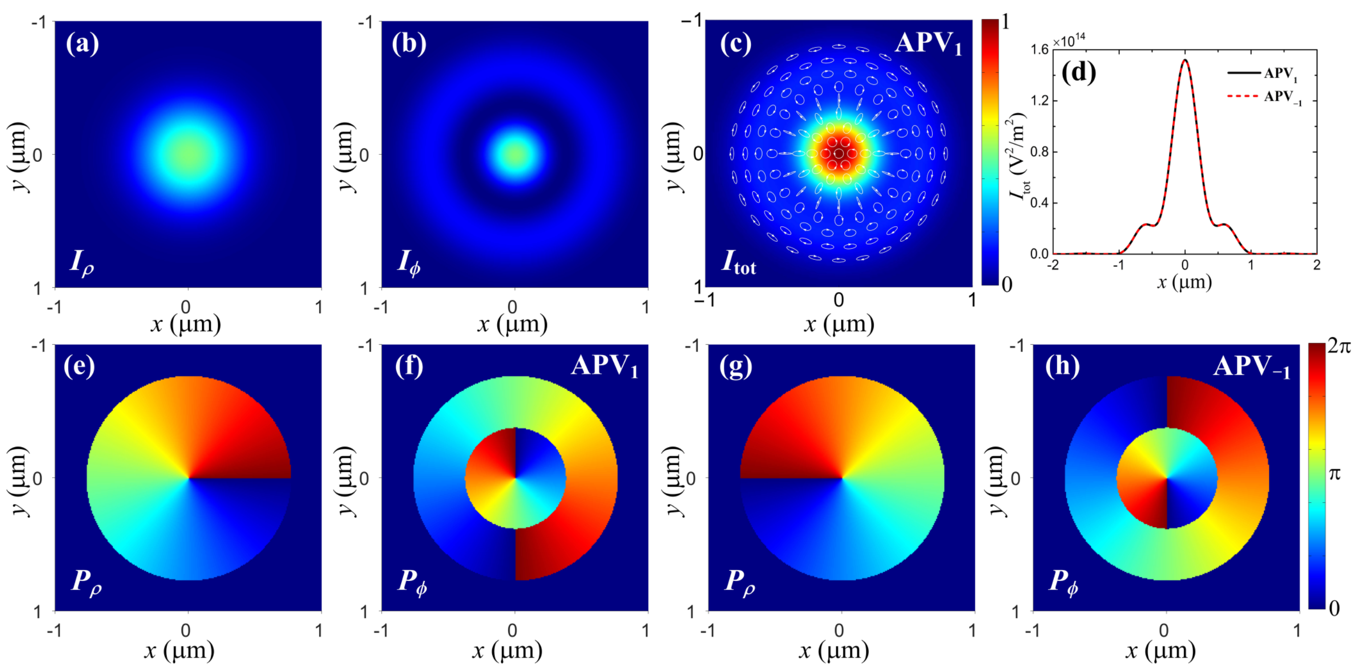

FIG. 2. (a)–(c) Intensity distributions in the focal plane of highly focused incident APV$_1$ beam.(d) Line scans along the x axis of the total intensity distributions. (e)–(h) Corresponding phase distributions of the radial and azimuthal field components in the focal plane for APV$_1$ (e) and (f), and APV$_{-1}$ (g) and (h) beams, respectively. The white circles with arrows in (c) indicate the local polarization ellipses.

the incident wavelength is $\lambda_0 = 1.064\,\mu$m, the image space refractive index $n_1 = 1.33$, and the ratio $\beta_0 = 1.5$. As shown in Fig. 1, the incident APV_1 beam has an annular intensity distribution and a polarization distribution along the azimuthal direction, and a vortex phase distribution. Shown in Figs. 2(a)–2(c) in turn are the intensity components I_ρ, I_ϕ, and the total intensity I_{tot} for the focused APV_1 beam. Different from focusing an AP beam where the intensity in the focal plane has a doughnut shape, the APV illumination with $m = 1$ generates a sharp focal spot. The local polarization ellipses of the focused field are plotted as shown in Fig. 2(c). Notice that the field is strictly circularly polarized in the focus and elliptically polarized away from the focus. When changing the topological charge $m = 1$ to -1, it finds that the intensity distributions have the same shape regardless of the sign of the topological charge. To clarify this further, both the total intensity distributions of the focused APV_1 and APV_{-1} along the x axis are plotted in Fig. 2(d). It is clearly seen that the intensities of the two cases are coincident completely. Shown in Figs. 2(e)–2(h) are the corresponding phase distributions, which are plotted in the region where the total intensity is greater than one-tenth of the peak intensity for the focused APV_1 and APV_{-1} beams. Here, P_ρ represents the phase of the radial electric-field component and similarly for P_ϕ. The periodic phase distributions along the azimuthal direction are evident, suggesting the presence of OAM in the focused field. Along the radial direction, P_ρ keeps constant while P_ϕ has a π-phase jump. The comparisons of the phase distributions between focused APV_1 and APV_{-1} beams manifest that the radial (azimuthal) field components have π-phase difference. Notice that the radial and azimuthal field components are $\pi/2$ out of phase, just as can be seen from Eq. (4).

III. ANGULAR MOMENTUM OF THE FOCUSING FIELDS

We now turn to the calculation of the AM of the focused field. The Minkowski form of the electromagnetic momentum density $\mathbf{g} = \varepsilon_1\mu_1(\mathbf{E}\times\mathbf{H})$, which is proportional to the energy flow described by the Poynting vector with $\mathbf{E}$ and $\mathbf{H}$ being the electric and magnetic fields, respectively, and ε_1 and μ_1 being the permittivity and permeability of medium, respectively, is adopted. Then the AM density $\mathbf{j}$ of the light beam can be expressed as [33]

$$\mathbf{j} = \mathbf{r}\times\mathbf{g} = \varepsilon_1\mu_1\mathbf{r}\times(\mathbf{E}\times\mathbf{H}), \tag{5}$$

which can be rewritten as $\mathbf{j} = \mathbf{L} + \mathbf{S}$ with $\mathbf{L}$ and $\mathbf{S}$ being, respectively, the orbital and spin parts. For monochromatic light beam with an angular frequency ω, and by adopting the electric-magnetic democracy or dual-symmetry formalism [34,35], the time-averaged OAM and SAM densities can be written as [36]

$$\langle\mathbf{L}\rangle = \frac{1}{4\omega}\mathrm{Im}[\varepsilon_1\mathbf{E}^*\cdot(\mathbf{r}\times\nabla)\mathbf{E} + \mu_1\mathbf{H}^*\cdot(\mathbf{r}\times\nabla)\mathbf{H}], \tag{6}$$

$$\langle\mathbf{S}\rangle = \frac{1}{4\omega}\mathrm{Im}[\varepsilon_1\mathbf{E}^*\times\mathbf{E} + \mu_1\mathbf{H}^*\times\mathbf{H}]. \tag{7}$$

Here the superscript * denotes the complex conjugate. Usually, in light-matter interactions, both the particle and the surrounding medium are nonmagnetic, such that the particle predominantly reacts to the electric part of the field [37]. Hence, we focus on the AMs originated from the electric-field part and the corresponding mechanical effects. For the orbital part according to Eq. (6), the focused field (4) has nonvanishing OAM density due to the vortex phase structure $\exp(im\phi_s)$, as also can be seen from Fig. 2. Where the spin part (7) is concerned, the term $\mathrm{Im}[\mathbf{E}^*\times\mathbf{E}]$ is not equal to zero, implying that the focused field carries the SAM density which is, of course, purely longitudinal. This is different from the azimuthally directed SAM occurring in the focused circular or radial polarization field [8].

The normalized longitudinal SAM density S_z and OAM density L_z of the focused APV_1 and APV_{-1} beams are plotted in Fig. 3. As a comparison, the cases of left- and right-hand circular polarization (LCP and RCP) beams are also shown. The magnitudes of the SAM densities dominate near the focus [upper row of Figs. 3(a)–3(d)], while those of the OAM densities exhibit annular distributions [lower row of Figs. 3(e)–3(h)]. Similar to focusing the CP beams where the orientations of S_z and L_z are in line with the handedness of circular polarization, those of the focused APV beams are controlled by the sign of the topological charge. At a fixed point, the orientation of S_z as well as L_z reverses when the sign of the topological charge is changed. In addition, the magnitudes in arbitrary units of the S_z and L_z along the x axis are plotted in Figs. 3(i) and 3(j); all values are normalized to the maximum of S_z and L_z of the focused CP case, respectively. The absolute magnitudes of both S_z and L_z remain unchanged when the topological charge changes from $m = 1$ to -1 for the focused APV beams, or the handedness changes from left- to right-hand for the focused CP beams. Note that the S_z for focused APV_1 (APV_{-1}) beam is in fact negative (positive) on the outer side of the ring of maximum intensity, while it reverses the sign on the inside. This arises directly from the phase change of the azimuthal component as shown in Fig. 2. Calculations present that the maximal absolute value of S_z for the focused APV beam is 0.83-fold that of the focused CP beam, while on the contrary, the maximal absolute value of L_z for the focused APV beam is much larger than that of the focused CP beam.

The aforementioned discussion shows that the focused field of the APV input has locally nonvanishing optical OAM as well as SAM densities. We now turn to calculate the global OAM and SAM of the focused field. In the nonparaxial regime, the total AM crossing some plane can be computed by evaluating the integral of the angular momentum tensor $\overleftrightarrow{\mathbf{M}} = \mathbf{r}\times\overleftrightarrow{\mathbf{T}}$, or in component form $M_{ij} = \sum_{kl}\varepsilon_{ikl}r_k T_{lj}$, where ε_{ikl} is the Levi-Civita symbol and $\overleftrightarrow{\mathbf{T}}$ is Maxwell stress tensor or called momentum flux density, defined as [33]

$$T_{ij} = \tfrac{1}{2}\delta_{ij}(\varepsilon_1 E^2 + \mu_1 H^2) - \varepsilon_1 E_i E_j - \mu_1 H_i H_j, \tag{8}$$

with δ_{ij} denoting the usual Kronecker delta. The z component of AM flux density M_{zz} can be expressed as

$$M_{zz} = \tfrac{1}{2}\mathrm{Re}[y(\varepsilon_1 E_x E_z^* + \mu_1 H_x^* H_z) - x(\varepsilon_1 E_y E_z^* + \mu_1 H_y^* H_z)]. \tag{9}$$

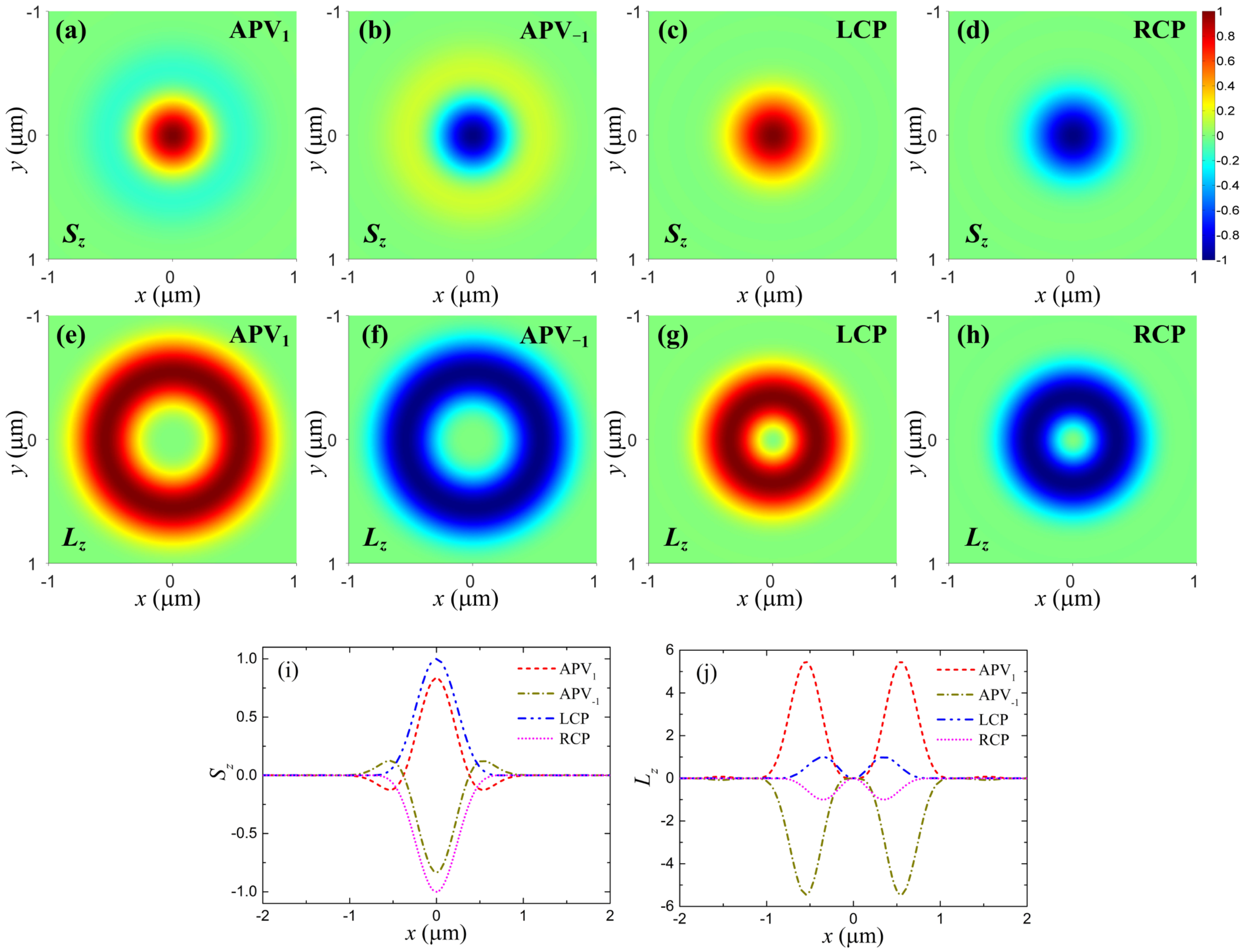

FIG. 3. Normalized longitudinal SAM and OAM density distributions in the focal plane for focused APV_1 (a) and (e); APV_{-1} (b) and (f); LCP (c) and (g); and RCP (d) and (h) beams, respectively. Line scans along the x axis of the normalized SAM (i) and OAM (j) densities.

According to Barnett [25], the M_{zz} can be separated into two gauge-independent contributions associated to the spatial field structure and to the polarization

$$M_{zz}^{\mathrm{orbit}} = \frac{1}{4\omega}\mathrm{Im}\left[E_y\frac{\partial H_x^*}{\partial\phi_s} - H_x^*\frac{\partial E_y}{\partial\phi_s} + H_y^*\frac{\partial E_x}{\partial\phi_s} - E_x\frac{\partial H_y^*}{\partial\phi_s}\right], \tag{10}$$

$$M_{zz}^{\mathrm{spin}} = \frac{1}{2\omega}\mathrm{Im}[E_xH_x^* + E_yH_y^*]. \tag{11}$$

Integrating the flux density over the whole xy plane yields the total AM flux through a plane of constant z_s

$$\mathcal{M}_{zz}^{\mathrm{orbit}} = \frac{2\pi}{\mu_1\omega^2}\mathrm{Re}\left[\int\{(m+1)Q_{m+1}^0Q_{m+1}^{1*} + (m-1)Q_{m-1}^0Q_{m-1}^{1*}\}\rho_s d\rho_s\right], \tag{12}$$

$$\mathcal{M}_{zz}^{\mathrm{spin}} = \frac{2\pi}{\mu_1\omega^2}\mathrm{Re}\left[\int(Q_{m-1}^0Q_{m-1}^{1*} - Q_{m+1}^0Q_{m+1}^{1*})\rho_s d\rho_s\right], \tag{13}$$

where the coefficients $Q_m^n (n = 0, 1)$ are

$$Q_m^n = C\int_0^{\vartheta}\cos^{1/2}\theta\sin\theta l(\theta)f_n(\theta)e^{ikz_s\cos\theta}J_m(\beta)d\theta, \tag{14}$$

with functions $f_0(\theta) = 1$ and $f_1(\theta) = k\cos\theta$. In order to identify the magnitude of the AM per photon, we need the energy flux through the plane which is, after integrating the time-averaged axial energy flux $1/2\mathrm{Re}(\mathbf{E}\times\mathbf{H}^*)_z$,

$$\mathcal{F}_z = \frac{2\pi}{\mu_1\omega}\mathrm{Re}\left[\int(Q_{m+1}^0Q_{m+1}^{1*} + Q_{m-1}^0Q_{m-1}^{1*})\rho_s d\rho_s\right]. \tag{15}$$

Given Eqs. (12), (13), and (15), it follows that

$$\frac{\mathcal{M}_{zz}^{\mathrm{orbit}} + \mathcal{M}_{zz}^{\mathrm{spin}}}{\mathcal{F}_z} = \frac{m}{\omega}. \tag{16}$$

From Eq. (16), it is seen that the focused field has total AM of $m\hbar$ per photon. This demonstrates that the total AM flux across any transverse plane is conserved.

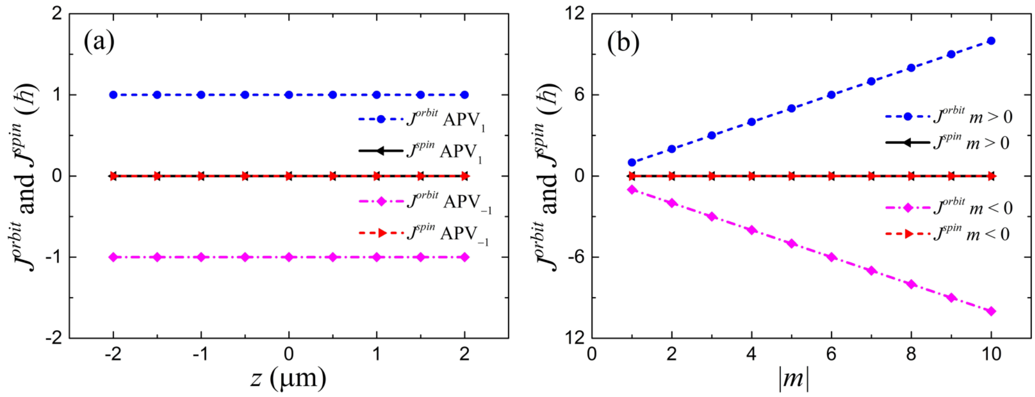

FIG. 4. Dependences of the total OAM and SAM per photon of the focused field on (a) the axial distances and (b) the topological charge of incident beam.

Accordingly, the orbital and spin components of AM per photon are given by

$$J^{\text{orbit}} = \frac{\mathcal{M}_{zz}^{\text{orbit}}}{\mathcal{F}_z/\hbar\omega}, \qquad J^{\text{spin}} = \frac{\mathcal{M}_{zz}^{\text{spin}}}{\mathcal{F}_z/\hbar\omega}. \tag{17}$$

Figure 4(a) plots the changes of the total OAM J^{orbit} and SAM J^{spin} per photon for incident APV_1 and APV_{-1} beams with axial distances. It shows that the total SAM is zero regardless of which transverse plane is considered. The dependences of the focal plane J^{orbit} and J^{spin} on the topological charge m of the incident beam are plotted in Fig. 4(b). Note that the total SAM of the focused field is always zero, while the OAM is equal to that of the incident beam. Combining these results and the above analysis show that the OAM of the incident APV beam is not converted to a global SAM of the focused field but induces a local distribution of the SAM.

IV. SPINNING OF PARTICLES IN THE FOCUSED FIELDS

Although a global SAM is absent, the mechanical effects on probe particles can be induced by the localized optical SAM. To illustrate this, we employ an absorptive particle to detect the local SAM. If it does exist, the particle should experience an optical torque along the axial direction and then spin around its own axis. Under the illuminations of either APV_1 or APV_{-1} beam (Fig. 2), the particle will be trapped on the beam axis as the intensity gradient [38]. However, due to the equivalence of the OAM and SAM densities when spinning a particle with size larger than the focal spot size, one cannot distinguish between the two AM densities unless the particle is small enough (Fig. 3). So, a Rayleigh spherical particle with radius of $a = 30\,\text{nm}$, which is much smaller than the trapping wavelength and being unaffected by the OAM density when trapped on the beam axis, is considered here. The particle, with permittivity ε_2, can be considered simply as an induced electric dipole. Then, the induced dipole moment is $\mathbf{p} = \alpha\mathbf{E}$, where α is the polarizability given by [39]

$$\alpha = \frac{\alpha_0}{1 - i(2/3)k^3\alpha_0}, \quad \alpha_0 = 4\pi\varepsilon_1 a^3 \frac{\varepsilon_2/\varepsilon_1 - 1}{\varepsilon_2/\varepsilon_1 + 2}. \tag{18}$$

In light-matter interaction, the transfer of optical AM from light beam to the particle induces an optical torque $\mathbf{\Gamma} = \mathbf{p} \times \mathbf{E}$. Therefore, the time-averaged optical torque is [40,41]

$$\langle \mathbf{\Gamma} \rangle = \frac{1}{2}|\alpha|^2 \text{Re}\left[\frac{1}{\alpha_0^*}\mathbf{E} \times \mathbf{E}^*\right]. \tag{19}$$

Considering the spherical particle with a refractive index of $n_2 = 1.59 + 0.005i$ illuminated by the focused APV_1 and APV_{-1} beams. Figure 5 shows the optical torque distributions experienced by the particle in the xz plane. It is clearly seen that the particle experiences a longitudinal optical torque indeed and undergoes a spin around the beam axis, or its own axis. With the topological charge $m = 1$, the spinning is along the positive z axis, while for $m = -1$ the spinning reverses the direction. Such a reversion is caused directly by the change of the orientation of the SAM density as shown

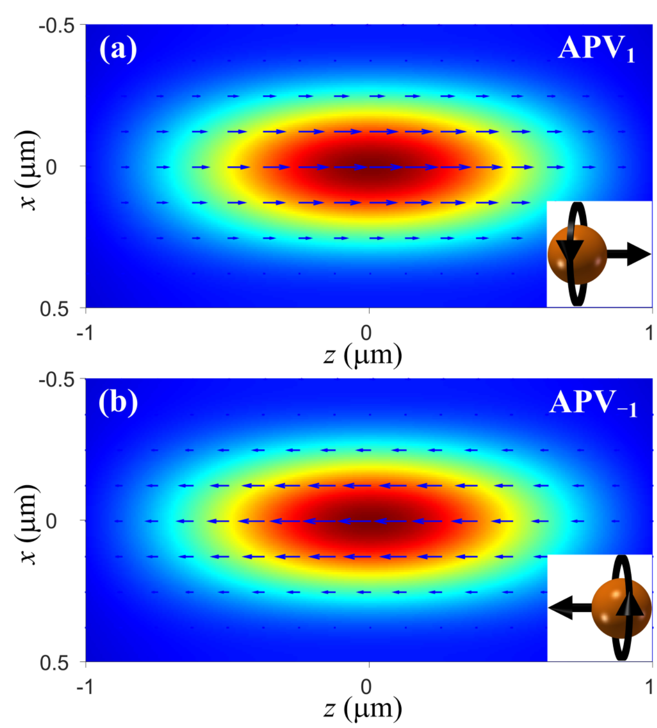

FIG. 5. Optical torque distributions experienced by the particle in the xz plane illuminated by highly focused (a) APV_1 and (b) APV_{-1} beams, respectively.

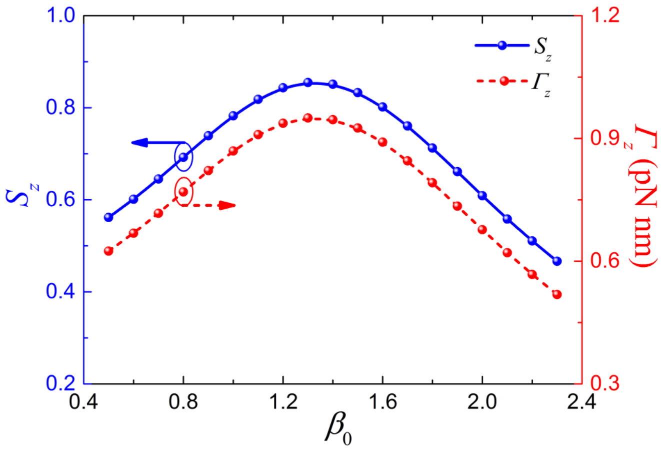

FIG. 6. Changes in the normalized longitudinal SAM density and optical torque with the ratio β_0 of the pupil radius to the beam waist under APV_1 illumination.

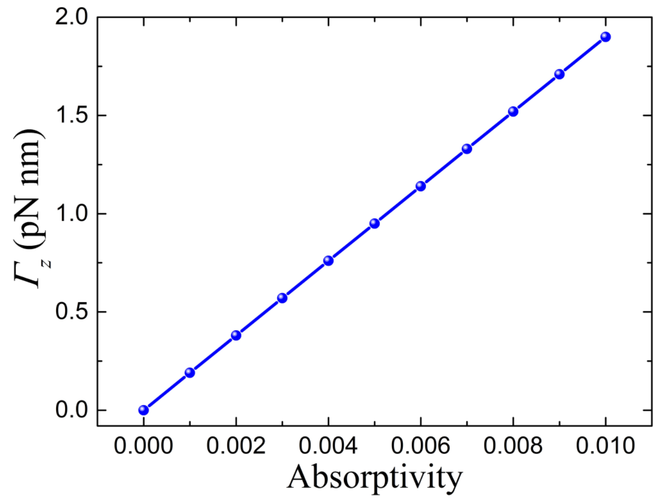

FIG. 7. Change in the longitudinal optical torque with the absorptivity of the particle under APV_1 illumination.

in Fig. 3, since optical torque $\langle \mathbf{\Gamma} \rangle \propto \mathrm{Re}[(1/\alpha_0^*)\mathbf{E} \times \mathbf{E}^*] \propto \mathrm{Im}[1/\alpha_0^*]\mathrm{Im}[\mathbf{E}^* \times \mathbf{E}]$, clearly showing that the torque exerted on the particle comes from the SAM transferred from light beam. Quantitatively, the longitudinal torque on the particle at the equilibrium position is $\Gamma_z = 0.93$ (or -0.93) pN nm for focused APV_1 (or APV_{-1}) beam. The cases for CP illuminations are also calculated, $\Gamma_z = 1.12$ (or -1.12) pN nm for focused LCP (or RCP) beam. The ratio of the torque between focused APV and CP is roughly 0.83, the same as that of the SAM density between both as mentioned above. Here lies the fact that the torque is proportional to the SAM density.

In all preceding calculations, the ratio β_0 of the pupil radius to the beam waist for the input field is set to 1.5. In this section, this value is variable. We may expect some changing results for the longitudinal SAM density S_z and optical torque Γ_z on varying the size of the ratio. In Fig. 6, it plots the curves of S_z, which is normalized to the maximum of S_z of the focused LCP case in Fig. 3(i), and Γ_z evaluated at the equilibrium position for APV_1 illumination as β_0 varies. With increasing the value of β_0, both S_z and Γ_z firstly increase until a peak is reached at $\beta_0 = 1.3$; thereafter, they decrease gradually. This demonstrates that the localized SAM is changeable, despite of the null global SAM. The similar variation tendency between the torque and the SAM density proves once again that the mechanical torque on the particle comes from the transferred localized SAM from the light beam. In short, the beam has an optimal ratio of the pupil radius to the beam waist corresponding to the maximum optical torque.

Finally, the effect of the absorptivity (characterized by the imaginary part of the refractive index) of the particle on the longitudinal torque Γ_z for APV_1 illumination is examined. In the calculation, the ratio β_0 takes the optimal value of 1.3 and the real part of the refractive index is held at 1.59. According to Fig. 7, as the absorption increases, the Γ_z increases in a simple linear relation, indicating that the magnitude of the torque can be increased further by increasing the absorptivity of the particle.

V. CONCLUSIONS

In conclusion, we have proposed and revealed that the incident OAM can affect the SAM distribution of the focused field in strong focusing of an APV beam. Such incident field that carries only OAM, through high focusing, generates a purely transverse electric field with $\pi/2$ phase difference between the radial and azimuthal field components, leading to the localized longitudinal SAM occurring in the focused field, which can be used to drive axial spinning of an absorptive Rayleigh particle. The sign of the topological charge of the input field determines both orientations of the SAM and OAM densities of the focused field as well as the spinning direction of the particle. The magnitudes of the localized SAM and optical torque can be controlled by adjusting the ratio β_0 of the input field, with both quantities attaining a maximum value at $\beta_0 = 1.3$. Moreover, the torque in magnitude can be increased by properly increasing the particle's absorptivity. This investigation provides a new degree of freedom for spinning particles by using a vortex phase, which may have considerable potentials in optical spin and orbit interaction, light-beam shaping, or optical manipulation.

ACKNOWLEDGMENTS

This research is supported by National Basic Research Program (973 Program) of China under Grant No. 2012CB921900, and the Natural Science Foundation of China (NSFC) under Grants No. 11474352, No. 61377008, and 11574389. We appreciate the reviewers' constructive and valuable comments and suggestions.

[1] L. Allen, S. M. Barnett, and M. J. Padgett, *Optical Angular Momentum* (Institute of Physics, Bristol, 2003).

[2] R. A. Beth, Mechanical detection and measurement of the angular momentum of light, Phys. Rev. **50**, 115 (1936).

[3] L. Allen, M. W. Beijersbergen, R. Spreeuw, and J. Woerdman, Orbital angular momentum of light and the transformation of Laguerre-Gaussian laser modes, Phys. Rev. A **45**, 8185 (1992).

[4] M. Friese, T. Nieminen, N. Heckenberg, and H. Rubinsztein-Dunlop, Optical alignment and spinning of laser-trapped microscopic particles, Nature (London) **394**, 348 (1998).

[5] A. Lehmuskero, R. Ogier, T. Gschneidtner, P. Johansson, and M. Käll, Ultrafast spinning of gold nanoparticles in water using circularly polarized light, Nano Lett. **13**, 3129 (2013).

[6] M. Li, S. Yan, Y. Liang, P. Zhang, and B. Yao, Transverse spinning of particles in highly focused vector vortex beams, Phys. Rev. A **95**, 053802 (2017).

[7] J. Ng, Z. Lin, and C. Chan, Theory of Optical Trapping by an Optical Vortex Beam, Phys. Rev. Lett. **104**, 103601 (2010).

[8] M. Li, S. Yan, B. Yao, Y. Liang, and P. Zhang, Spinning and orbiting motion of particles in vortex beams with circular or radial polarizations, Opt. Express **24**, 20604 (2016).

[9] R. Paez-Lopez, U. Ruiz, V. Arrizon, and R. Ramos-Garcia, Optical manipulation using optimal annular vortices, Opt. Lett. **41**, 4138 (2016).

[10] D. G. Grier, A revolution in optical manipulation, Nature (London) **424**, 810 (2003).

[11] M. Padgett and R. Bowman, Tweezers with a twist, Nat. Photonics **5**, 343 (2011).

[12] J. Lipfert, M. M. van Oene, M. Lee, F. Pedaci, and N. H. Dekker, Torque spectroscopy for the study of rotary motion in biological systems, Chem. Rev. **115**, 1449 (2015).

[13] M. Aspelmeyer, T. J. Kippenberg, and F. Marquardt, Cavity optomechanics, Rev. Mod. Phys. **86**, 1391 (2014).

[14] V. Liberman and B. Y. Zel'dovich, Spin-orbit interaction of a photon in an inhomogeneous medium, Phys. Rev. A **46**, 5199 (1992).

[15] L. Marrucci, C. Manzo, and D. Paparo, Optical Spin-to-Orbital Angular Momentum Conversion in Inhomogeneous Anisotropic Media, Phys. Rev. Lett. **96**, 163905 (2006).

[16] N. Shitrit, I. Yulevich, E. Maguid, D. Ozeri, D. Veksler, V. Kleiner, and E. Hasman, Spin-optical metamaterial route to spin-controlled photonics, Science **340**, 724 (2013).

[17] K. Y. Bliokh, E. A. Ostrovskaya, M. A. Alonso, O. G. Rodríguez-Herrera, D. Lara, and C. Dainty, Spin-to-orbit angular momentum conversion in focusing, scattering, and imaging systems, Opt. Express **19**, 26132 (2011).

[18] V. Sala, D. Solnyshkov, I. Carusotto, T. Jacqmin, A. Lemaître, H. Terças, A. Nalitov, M. Abbarchi, E. Galopin, and I. Sagnes, Spin-Orbit Coupling for Photons and Polaritons in Microstructures, Phys. Rev. X **5**, 011034 (2015).

[19] K. Y. Bliokh, F. Rodríguez-Fortuño, F. Nori, and A. V. Zayats, Spin-orbit interactions of light, Nat. Photonics **9**, 796 (2015).

[20] F. Cardano and L. Marrucci, Spin-orbit photonics, Nat. Photonics **9**, 776 (2015).

[21] C. P. Jisha, and A. Alberucci, Spin-orbit interactions in optically active materials, Opt. Lett. **42**, 419 (2017).

[22] Y. Zhao, J. S. Edgar, G. D. Jeffries, D. McGloin, and D. T. Chiu, Spin-to-Orbital Angular Momentum Conversion in a Strongly Focused Optical Beam, Phys. Rev. Lett. **99**, 073901 (2007).

[23] E. Brasselet, N. Murazawa, H. Misawa, and S. Juodkazis, Optical Vortices from Liquid Crystal Droplets, Phys. Rev. Lett. **103**, 103903 (2009).

[24] F. J. Rodríguez-Fortuño, G. Marino, P. Ginzburg, D. O'Connor, A. Martínez, G. A. Wurtz, and A. V. Zayats, Near-field interference for the unidirectional excitation of electromagnetic guided modes, Science **340**, 328 (2013).

[25] S. M. Barnett, Optical angular-momentum flux, J. Opt. B: Quantum Semiclass. Opt. **4**, S7 (2002).

[26] P. B. Monteiro, P. A. M. Neto, and H. M. Nussenzveig, Angular momentum of focused beams: Beyond the paraxial approximation, Phys. Rev. A **79**, 033830 (2009).

[27] X. Hao, C. Kuang, T. Wang, and X. Liu, Phase encoding for sharper focus of the azimuthally polarized beam, Opt. Lett. **35**, 3928 (2010).

[28] W. Zhang, S. Liu, P. Li, X. Jiao, and J. Zhao, Controlling the polarization singularities of the focused azimuthally polarized beams, Opt. Express **21**, 974 (2013).

[29] X. Li, P. Venugopalan, H. Ren, M. Hong, and M. Gu, Super-resolved pure-transverse focal fields with an enhanced energy density through focus of an azimuthally polarized first-order vortex beam, Opt. Lett. **39**, 5961 (2014).

[30] B. Richards and E. Wolf, Electromagnetic diffraction in optical systems. II. Structure of the image field in an aplanatic system, Proc. R. Soc. Ser. A **253**, 358 (1959).

[31] K. S. Youngworth and T. G. Brown, Focusing of high numerical aperture cylindrical-vector beams, Opt. Express **7**, 77 (2000).

[32] Q. Zhan, Cylindrical vector beams: From mathematical concepts to applications, Adv. Opt. Photonics **1**, 1 (2009).

[33] J. D. Jackson, *Classical Electrodynamics*, 3rd ed. (John Wiley & Sons, New York, 1999).

[34] M. V. Berry, Optical currents, J. Opt. A: Pure Appl. Opt. **11**, 094001 (2009).

[35] K. Y. Bliokh, A. Y. Bekshaev, and F. Nori, Dual electromagnetism: helicity, spin, momentum and angular momentum, New J. Phys. **15**, 033026 (2013).

[36] A. Aiello, P. Banzer, M. Neugebauer, and G. Leuchs, From transverse angular momentum to photonic wheels, Nat. Photonics **9**, 789 (2015).

[37] K. Y. Bliokh, A. Y. Bekshaev, and F. Nori, Extraordinary momentum and spin in evanescent waves, Nat. Commun. **5**, 3300 (2014).

[38] A. Ashkin, J. Dziedzic, J. Bjorkholm, and S. Chu, Observation of a single-beam gradient force optical trap for dielectric particles, Opt. Lett. **11**, 288 (1986).

[39] B. T. Draine, The discrete-dipole approximation and its application to interstellar graphite grains, Astrophys. J. **333**, 848 (1988).

[40] M. Li, S. Yan, B. Yao, M. Lei, Y. Yang, J. Min, and D. Dan, Intrinsic optical torque of cylindrical vector beams on Rayleigh absorptive spherical particles, J. Opt. Soc. Am. A **31**, 1710 (2014).

[41] A. Canaguier-Durand, A. Cuche, C. Genet, and T. W. Ebbesen, Force and torque on an electric dipole by spinning light fields, Phys. Rev. A **88**, 033831 (2013).